Li *et al. Microstructures* **2025**, *5*, 2025033
DOI: 10.20517/microstructures.2024.114

Microstructures

Research Article

Open Access

Enabling highly reversible Zn anode via an interfacial preferentially adsorbed additive containing nucleophilic groups

Canglong Li[1,2], Hongli Qi[3], Jie Huang[4], Dongping Chen[3], Yuanzi Cheng[2], Minghan Xu[5], Zihao Jiang[6], Huaming Yu[2,7], Yang Huang[7], Guanghui Li[1], Yuejiao Chen[2]

[1]School of Minerals Processing and Bioengineering, Central South University, Changsha 410083, Hunan, China.
[2]State Key Laboratory of Powder Metallurgy, Central South University, Changsha 410083, Hunan, China.
[3]School of Chemistry and Chemical Engineering, Harbin Institute of Technology, Harbin 150001, Heilongjiang, China.
[4]National-Local Joint Engineering Laboratory of Marine Mineral Resources Exploration Equipment and Safety Technology, Hunan University of Science and Technology, Xiangtan 411201, Hunan, China.
[5]School of Materials Science and Engineering, Changchun University, Changchun 130022, Jilin, China.
[6]South China Advanced Institute for Soft Matter Science and Technology, School of Emergent Soft Matter, South China University of Technology, Guangzhou 510640, Guangdong, China.
[7]Thrust of Advanced Materials, The Hong Kong University of Science and Technology (Guangzhou), Guangzhou 511400, Guangdong, China.

Correspondence to: Dr. Huaming Yu, State Key Laboratory of Powder Metallurgy, Central South University, No. 932 Lushan South Road, Changsha 410083, Hunan, China; Thrust of Advanced Materials, The Hong Kong University of Science and Technology (Guangzhou), Guangzhou 511400, Guangdong, China. E-mail: hmYu147@outlook.com or hyu176@connect.hkust-gz.edu.cn; Prof. Yuejiao Chen, State Key Laboratory of Powder Metallurgy, Central South University, No. 932 Lushan South Road, Changsha 410083, Hunan, China. E-mail: cyj.strive@csu.edu.cn

How to cite this article: Li, C.; Qi, H.; Huang, J.; Chen, D.; Cheng, Y.; Xu, M.; Jiang, Z.; Yu, H.; Huang, Y.; Li, G.; Chen, Y. Enabling highly reversible Zn anode via an interfacial preferentially adsorbed additive containing nucleophilic groups. *Microstructures* **2025**, *5*, 2025033. https://dx.doi.org/10.20517/microstructures.2024.114

Received: 4 Nov 2024 **First Decision:** 4 Dec 2024 **Revised:** 6 Dec 2024 **Accepted:** 13 Dec 2024 **Published:** 21 Mar 2025

Academic Editors: Yida Deng, Nana Wang **Copy Editor:** Fangling Lan **Production Editor:** Fangling Lan

Abstract

The cyclability and reversibility of aqueous zinc-ion batteries (AZIBs) are severely hampered by the safety concerns arising from the Zn dendrite growth. Therefore, a stable anode with inhibited dendrites and side reactions is crucial for AZIBs. Herein, we utilized methyl acetoacetate (MA) as an additive to prevent dendrite growth and enable highly reversible Zn anodes. Benefiting from the nucleophilic groups (carbonyl groups) in MA, MA molecules can preferentially adsorb on the anode/electrolyte interface (AEI), forming a molecular protective layer. Such MA layers can not only regulate the migration and deposition of zinc ions, but also inhibit side reactions induced by the decomposition of free H_2O molecules at AEI. Therefore, the symmetric cell with the addition of MA

achieves a long-term cycling stability of 1,500 h at 2 mA cm^{-2} with a capacity of 2 mAh cm^{-2}. In addition, the Zn//NVO full cell using MA-contained electrolyte demonstrates a high specific capacity (138.4 mAh g^{-1}) with an outstanding capacity retention (92.8% after 600 cycles) at 1 A g^{-1}. This work provides a principle for the use of ester-based additives with nucleophilic groups to suppress Zn dendrite growth for highly durable zinc metal anodes.

Keywords: Zn anodes, aqueous zinc-ion batteries, ester-based additive, nucleophilic groups, electrolyte optimization

INTRODUCTION

Currently, constructing a cleaner and more efficient society requires greater utilization of renewable energy sources to replace fossil fuels[1-3]. Due to the unstable nature of renewable energy, there is an urgent need to develop large-scale electrochemical energy storage systems (ESS) to cope with grid fluctuations[4-7]. Considering the strict requirements for safety and economy, aqueous zinc-ion batteries (AZIBs) are considered the most promising alternatives for grid energy storage. The Zn anode possesses core advantages including environmental friendliness, low cost, high energy density (820 mAh g^{-1}), and appropriate redox potential (-0.76 V *vs.* the standard hydrogen electrode)[8-11]. However, the cycle lifespan of the zinc metal anode is seriously insufficient to satisfy the demands of commercial application, which is owing to the numerous complex reactions occurring at the interface of zinc metal anode in aqueous electrolytes[12,13]. It is well known that during electrodeposition, the Zn anode undergoes uneven initial nucleation of zinc. Under the "tip effect", zinc dendrites grow rapidly, eventually piercing the separator and causing a sudden short circuit[14-16]. In addition, the Zn anode is in a thermodynamically unstable state in aqueous solutions, where active water molecules in the electrolyte can compete with Zn^{2+} cations to capture electrons, leading to a hydrogen evolution reaction (HER)[17-19]. The occurrence of HER is accompanied by a local increase in pH at the anode surface, which in turn leads to surface hydroxide sulfate passivation. Dendrite growth and parasitic side reactions resonate with each other, severely limiting the practicality of AZIBs as a feasible and effective ESS.

The deposition morphology and uniformity of zinc are determined by the deposition/dissolution behavior of Zn[20,21]. Altering the chemical environment at the surface of zinc metal and regulating the distribution and transport of Zn^{2+} at the anode/electrolyte interface (AEI) are key to continuously optimizing the morphological evolution of the zinc metal anode[22-24]. Unlike traditional methods of constructing an artificial solid electrolyte interface (SEI) on zinc metal to regulate the deposition kinetics of Zn^{2+}, the use of electrolyte optimization strategies has been proven to be a simple and direct approach to control the deposition behavior of Zn^{2+}[25,26]. Some organic compounds containing polar groups, such as alcohols, ketones, and ethers, can optimize the deposition behavior of zinc and suppress side reactions by altering the solvation structure of zinc ions or reconstructing the hydrogen bonding network in the electrolyte[27,28]. Recently, ester-based organic molecules, due to their strong adsorption capacity for zinc, have been used to regulate the interfacial chemistry of the zinc metal anode[29]. For example, Wang *et al.* used the interaction of trimethyl phosphate (TMP) molecules to increase the electron density of water protons, thereby suppressing water activity and enabling symmetrical cells to operate for up to 1,600 h[3]. Liu *et al.* constructed a mixture solvent using propylene carbonate (PC) and aqueous solution, effectively reducing the free water molecules in the Zn^{2+}-solvent cations, enabling the full cells to exhibit a high specific capacity of 183 mAh g^{-1} over 300 cycles[30]. However, current research on ester components mostly involves adding them as co-solvents to aqueous electrolytes, which significantly increases the cost of the electrolyte and decreases the ionic conductivity. Therefore, exploring the use of ester molecules in trace addition, and elucidating the

underlying mechanisms by which ester molecules regulate the zinc deposition process is crucial for the application of ester organic compounds in AZIBs.

In this study, we present methyl acetoacetate (MA), a water-soluble ester, as a novel additive for AZIBs to improve the stability and reversibility of zinc electrodes. The calculated and experimental results indicate that the MA molecule possesses two oxygen atoms with high charge density, which can preferentially adsorb at AEI, effectively controlling the nucleation and diffusion processes of zinc ions. This molecular adsorption layer also promotes the growth of the preferred Zn (002) crystal facet and limits the generation of zinc dendrites. Furthermore, the adsorbed MA molecules create an electrical double layer (EDL) with reduced water content at AEI. This unique water-poor EDL prevents direct contact between zinc foils and active H_2O, restraining the Zn corrosion reaction [Scheme 1]. As a consequence, modulated Zn deposition behaviors by MA additives greatly prolong the cycling lifespan of symmetric cells over 1,500 h (2 mA cm^{-2} with a capacity of 2 mAh cm^{-2}) and the Zn//Cu cell achieves stable cycling for 1,400 cycles at 2 mA cm^{-2}. Moreover, at 1 A g^{-1}, the Zn//NVO full cell using MA exhibits an improved reversible specific capacity retention of 92.8% after 600 cycles. This research offers a guideline of utilizing ester-based additives to enable highly reversible Zn anodes for high-performance AZIBs.

MATERIALS AND METHODS

Electrolyte preparation

The process of making an electrolyte includes dissolving $ZnSO_4·7H_2O$ (99.995%, Aladdin) in deionized (DI) water to prepare a solution of 2 M $ZnSO_4$. To produce an electrolyte with MA, MA of 99% purity from Aladdin was incorporated into the 2 M $ZnSO_4$ solution. Additionally, $Zn(CF_3SO_3)_2$ (98.0%, Aladdin) was utilized for the full cells.

Synthesis of cathode $Na_5V_{12}O_{32}$ (NVO) powders

First, 1.819 g V_2O_5 and 0.400 g NaOH were dissolved into 40 mL DI water and the mixed solution was stirred continuously for 30 min. Following that, the mixture was introduced into a 50 mL pressure vessel and maintained at a temperature of 180 °C for a duration of 48 h. The precursors were collected after repeatedly washing and centrifuging, and dried at 80 °C under vacuum conditions for 12 h. The precursors were heated in air for 2 h at 300 °C to finally obtain $Na_5V_{12}O_{32}$ (NVO) powder.

Material characterization

Scanning electron microscopy (SEM) images of sample morphology were analyzed via TESCAN. The morphology of the surface of the anodes after cycling was examined using laser confocal microscopy (KEYENCE VK-X150). Raman microscopy (Thermo Scientific DXR3) using 532 nm lasers, while the Smartlab SE instrument was used for X-ray diffraction (XRD) analysis with a step size of 0.02° to check the crystal structure. X-ray photoelectron spectroscopy (XPS) tests were conducted to study the valence state of each element (Thermo Scientific K-Alpha). The contact angles of various electrolytes on the electrode surface are measured using a contact angle tester (DINGSHENG JY-82C).

Electrochemical characterization

The assembly of the cells was conducted in CR2025 coin-type cells under ambient air conditions. The glass fiber separator (Whatman, GF-D) was employed. The electrolyte for both asymmetric and symmetric cells was a standard 2 M aqueous solution of $ZnSO_4$. The full cell utilized a 2 M $Zn(CF_3SO_3)_2$ electrolyte. The NEWARE battery-testing system (MIHW-200-160CH-B, Shenzhen, China) was used to perform extended cycling and rate capability tests at an ambient temperature of 25 °C. Electrochemical characterization, including impedance spectroscopy [electrochemical impedance spectroscopy (EIS)] spanning from 100 kHz to 0.1 Hz and cyclic voltammetry (CV), was conducted with an electrochemical workstation (Ivium, Netherlands). For cathode fabrication, N-methylpyrrolidone (NMP) served as the solvent. The cathode

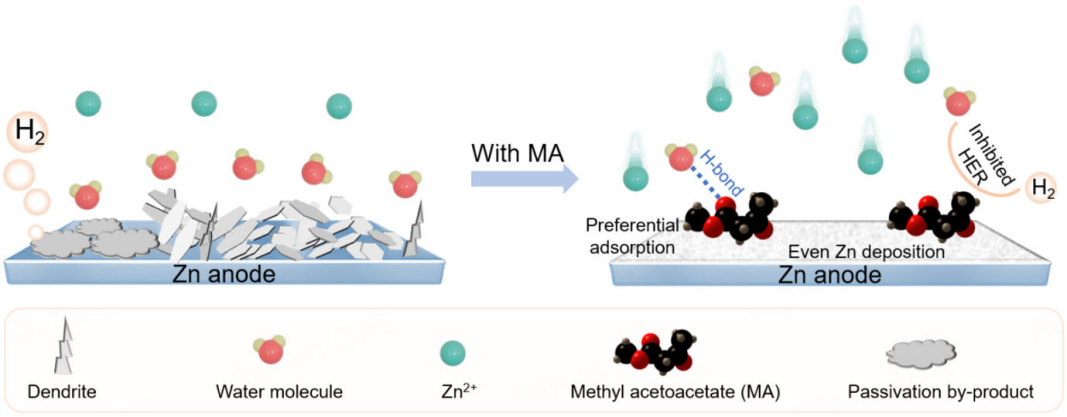

Scheme 1. Zn plating behavior under the effect of MA additive.

material, polyvinylidene fluoride and carbon black were mixed in a weight ratio of 7:2:1 using NMP as a solvent to create a slurry. This mixture was evenly coated onto a 20 μm thick titanium steel foil. Following the coating process, the foil underwent drying at 80 °C for a period of 12 h.

Simulation method

The electrostatic potential (ESP) and binding energy were calculated using the Gaussian 09 software. The geometries of the molecules were optimized employing the B3LYP hybrid functional in conjunction with the 6-31G+ basis sets. The ESP diagrams were generated using Multiwfn 3.8 software. Atomic models and ESP diagrams were visualized with VMD19 software, utilizing an iso-surface value of 0.03 for clarity. In addition, the DFT-D3 dispersion correction methods were implemented to accurately represent the subtle interactions from cations to anions.

The computational tool VASP was utilized to determine the charge distribution and the density of states (DOS) for the studied systems, adhering to the principles of density functional theory (DFT). The generalized gradient approximation (GGA), specifically the Perdew-Burke-Ernzerhof (PBE) functional, was applied to calculate the exchange-correlation energy. A plane-wave basis set with an energy cutoff of 450 eV was implemented to achieve accurate self-consistent charge density calculations. The convergence criterion for atomic forces was set at 0.01 eV $Å^{-1}$, which is crucial for determining the equilibrium geometries. The surface slab model was meticulously constructed, incorporating a generous vacuum space of 30 Å to preclude interactions between distinct slabs. The sampling of the Brillouin zone was conducted with a 2 × 2 × 1 Monkhorst-Pack grid for the optimization of atomic structures. The DFT-D3 method, accounting for dispersion forces, was implemented to analyze the intricate interactions between the slabs and the reactive species. The adsorption energy (E_{ads}) of the system was determined using

$$E_{ads} = E_{total} - E_a - E_b$$

where E_a or E_b is the energy of Zn bulk and adsorbent, and E_{total} is the total energy of the system.

RESULTS AND DISCUSSION

The molecular structure of MA with two nucleophilic carbonyl groups is shown in Figure 1A. The surface ESP is utilized to investigate the contribution of MA molecules to electrochemical processes. As displayed in Figure 1B, the results evidence that electronegative carbonyl oxygen atoms in MA molecules exhibit more

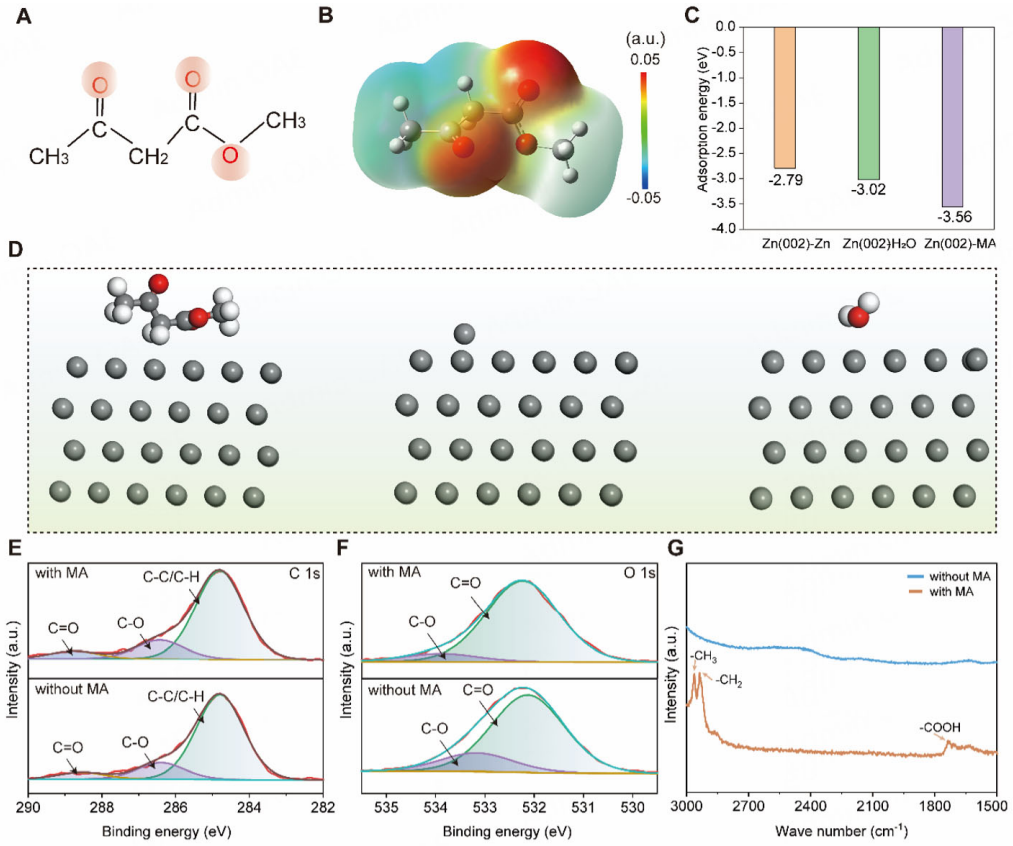

Figure 1. (A) Molecular structure and (B) electrostatic potential mapping of MA. (C) The adsorption energy of the zinc atom, water molecule and MA molecule on Zn (002) crystal plane. The corresponding structures of the (D) MA molecule, Zn atom and water molecule adsorbed on zinc. (E) C 1s, (F) N 1s XPS spectrum, and (G) Raman spectra of zinc foils immersed in electrolyte with/without MA for 5 days.

negative ESP value than other atoms, suggesting that zinc metal anode and positively charged Zn^{2+} ions interact more strongly with nucleophilic carbonyl groups on MA. This interaction favors the adsorption of MA onto the zinc foil surface in the electrolyte, thus modulating the distribution, transmission, and deposition dynamics of Zn^{2+} at the AEI. To explore the adsorption behavior of MA on zinc anode, the Eads of MA molecules, Zn atoms and H_2O molecules on the Zn (002) crystal plane was investigated via DFT calculations [Figure 1C], and the corresponding optimized structures are presented in Figure 1D. MA molecules demonstrate an Eads of -3.56 eV on the Zn (002) plane, which is much lower than that of Zn atoms (-2.79 eV) and H_2O molecules (-3.02 eV), proving the domain occupation of MA at AEI, which manipulates the kinetics of Zn^{2+} ions and reduces the proportion of adsorbed water molecule. In addition, the elemental composition and functional groups on the electrode reveal the adsorption of MA in XPS characterization and Raman spectrum. Supplementary Figure 1 shows the full survey spectra of the zinc foils soaked in different electrolytes for five days. In the high-resolution C 1s spectra [Figure 1E], C-C, C-O and C=O species can be detected for the zinc metal anode soaked in the solution with MA. Besides, the O 1s spectra in Figure 1F show a higher proportion of characteristic peaks of C=O and C-O bonds, which verify the presence of MA molecules on the anode surface. As depicted in the Raman spectra [Figure 1G], the characteristic peaks of MA can be observed for the zinc foil soaked in MA-contained electrolyte, where the $-CH_3$ band at 2,963 cm^{-1}, $-CH_2$ at 2,935 cm^{-1}, and -COOH at 1,735 cm^{-1} are consistent with the molecular structure of MA, indicating the strong adsorption between the MA molecules and zinc anode surfaces.

Because an electrolyte with 10 mM MA can maximize the cycling life of symmetric cells, this concentration of MA additives was selected as the optimal condition for the optimized electrolyte [Supplementary Figure 2]. Furthermore, some basic kinetics of interfacial stability for the electrolyte were conducted. First, the contact angle measurements were executed. As displayed in Figure 2A, with the addition of MA, the contact angle is reduced. This result demonstrates that the MA molecules significantly influenced the AEI and enhanced the wettability to the anode, which is crucial for achieving a uniform distribution of zinc ions. The nucleation overpotential is inherently connected to the formation of critical atom clusters. In Figure 2B, the overpotential for zinc nucleation at the zinc electrode in the MA-containing electrolyte is markedly higher than that observed in pure $ZnSO_4$ electrolyte. This indicates a substantial driving force that favors the formation of finer Zn nuclei and a greater nuclei density, which is further supported by the collected CV curves of symmetric cells using different electrolytes [Figure 2C]. It is generally believed that the formation of fine Zn nuclei is beneficial for homogeneous and dense Zn deposition, which can further enhance the cycling stability of zinc electrodes[31,32]. The coulombic efficiency (CE) value is used to characterize the reversibility of zinc anode during repeated deposition/dissolution processes. As presented in Figure 2D and E, at 6 mA cm^{-2}, the Zn//Cu asymmetric cell with MA maintains a higher and more stable CE in 800 cycles. On the contrary, in the electrolyte without MA, regular deposition/dissolution can only sustain less than 110 cycles. After 100 cycles, the voltage profile becomes erratic and the CE drops dramatically, indicating the presence of an internal short circuit [Supplementary Figure 3]. Additionally, the Zn//Cu asymmetric battery using MA-contained electrolyte performs steadily for over 1,400 cycles [Figure 2F] at a lower current density of 2 mA cm^{-2}. These results indicate that the stability and reversibility of zinc deposition/dissolution are significantly enhanced.

We believe that the nucleophilic carbonyl groups in MA act as an excellent hydrogen bond acceptor. Consequently, when MA molecules are adsorbed onto the Zn electrode surface, they can establish a MA-H_2O H-bond network. This network would confine water molecules and restrict their intermolecular interactions, thereby reducing water activity and restraining the decomposition of water[33,34]. To confirm this hypothesis, we conducted further analysis using Fourier transform infrared (FTIR) spectroscopy to track the evolution of hydrogen bonds within the electrolyte and to assess the ability of MA to inhibit corrosion of anode. As shown in the FTIR spectra [Figure 3A-C], the introduction of MA results in a redshift of the H-O stretching vibrations at 3,000-3,400 cm^{-1}. This shift signifies a coordination interaction between H_2O and MA, weakening the H-bond network among H_2O molecules. As a result, the number of active H_2O molecules can be reduced, which in turn suppresses parasitic reactions triggered by decomposition of water. Simultaneously, the addition of MA causes a noticeable blue shift in the stretching vibration of SO_4^{2-} at approximately 1,100 cm^{-1} in the FTIR spectra, which suggests a weaker interaction between Zn^{2+} and SO_4^{2-} mediated by MA[35-37]. In addition, the linear sweep voltammetry (LSV) curves [Figure 3D] provide clear insights into the HER performance. The addition of MA causes a negative shift in the current response, which confirms the inhibition of H_2 evolution. Typically, Zn electrodes exist in a thermodynamically unstable state within aqueous solutions, leading to continuous chemical corrosion. This corrosion process results in electrode passivation, which in turn diminishes the electrical conductivity[38-40]. Corrosion suppression capability of MA additive is also validated by immersing zinc foils in electrolytes with/without MA [Figure 3E and Supplementary Figure 4]. After only 5 days of immersion in a blank electrolyte, the Zn electrode becomes dark and turns from silvery white into black. As certified by the SEM images, it shows an extremely bumpy surface with an accumulation of uneven flakes. Conversely, the surface of the zinc electrode soaked in MA-contained electrolyte remains flat with a metallic luster, and only a few nanoparticles are visible in the SEM image. Furthermore, XRD patterns were utilized to examine the composition of by-products at the zinc foil surfaces. As illustrated in Supplementary Figure 5, the loosely and haphazardly accumulated flake layers are identified as primarily $Zn_4SO_4(OH)_6{\cdot}5H_2O$ by-product, and the Zn anode exhibits significantly stronger diffraction intensity in the MA-free electrolyte. During the

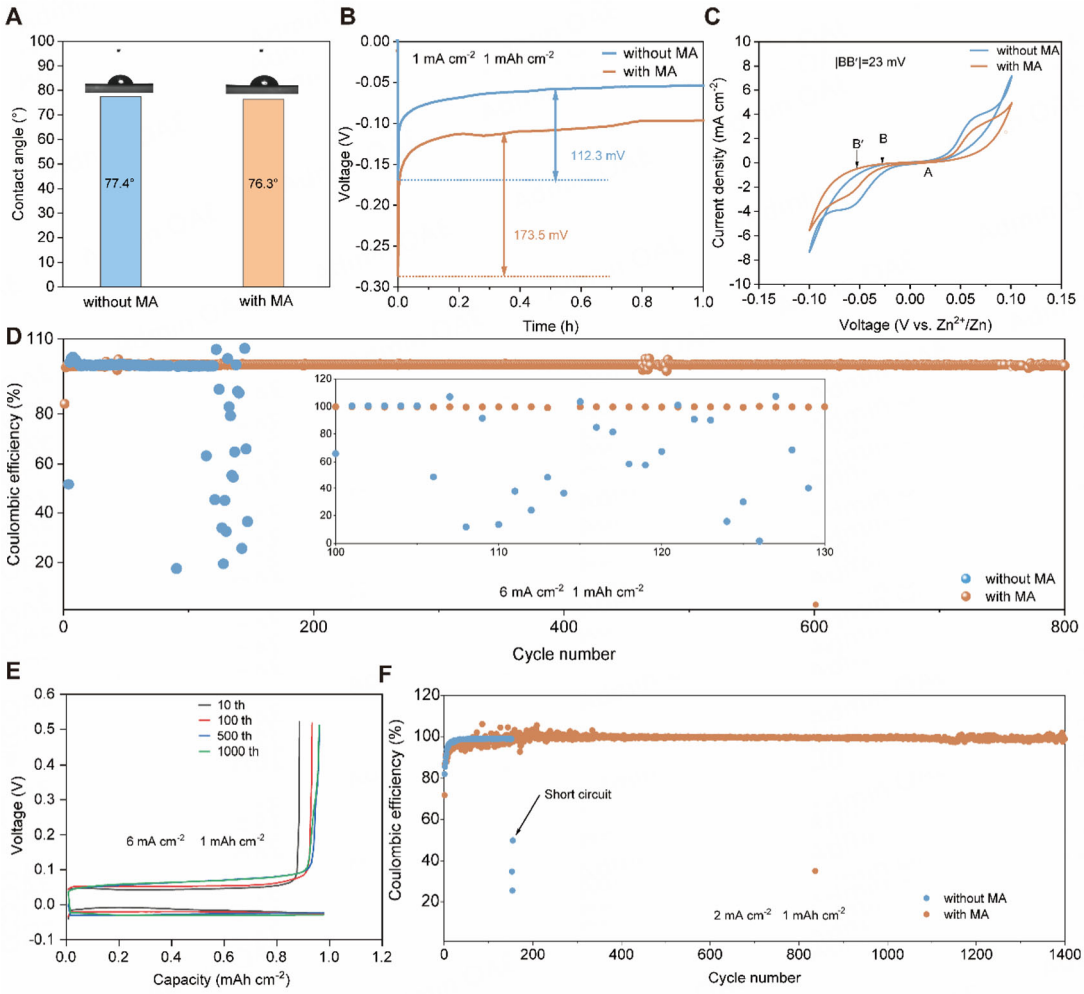

Figure 2. (A) Contact angle measurements of different electrolytes on zinc metal foil. (B) Nucleation overpotential at 1 mA cm^{-2} using different electrolytes. (C) CV curves of symmetric cells in different electrolytes. CE of asymmetric cells in different electrolytes at (D) 6 mA cm^{-2} and (F) 2 mA cm^{-2}. (E) Voltage profiles of Zn//Cu asymmetric cell with MA at 6 mA cm^{-2}.

cycling process, due to the coexistence of electrochemical corrosion and chemical corrosion, the corrosion on the anode surface will be more severe[41-43]. It is generally assumed that among the various crystal planes in the hexagonal close-packed structure, the (002) plane is advantageous for the even deposition of Zn^{2+} ions along a horizontal direction[44,45]. This crystal plane can also enhance the corrosion resistance of the anode and help curb the HER. Therefore, we also used XRD to detect the zinc electrodes after cycling in various electrolytes. As displayed in Figure 3F, the intensity ratios of (002) peak to (101) peak are 1.54 and 2.75 for Zn anode cycled in blank and MA-contained electrolyte, respectively, suggesting the increased (002) planes for zinc deposits in electrolyte with MA. Hydrogen evolution and surface passivation are common occurrences in batteries, whether during periods of inactivity or operation. To assess this, we evaluated the shelf life and recovery performance of symmetric cells under a regimen of alternating cycling and resting, as displayed in Figure 3G. The Zn//Zn cell using MA-contained electrolyte maintains stable electrochemical cycling for 2,500 h. On the contrary, the cell using the blank electrolyte shows substantial polarization voltage fluctuations, resulting in cell failure less than 200 h. Thus, the addition of MA can significantly stabilize the zinc metal electrode in aqueous electrolytes by reducing water activity and suppressing the Zn corrosion reaction.

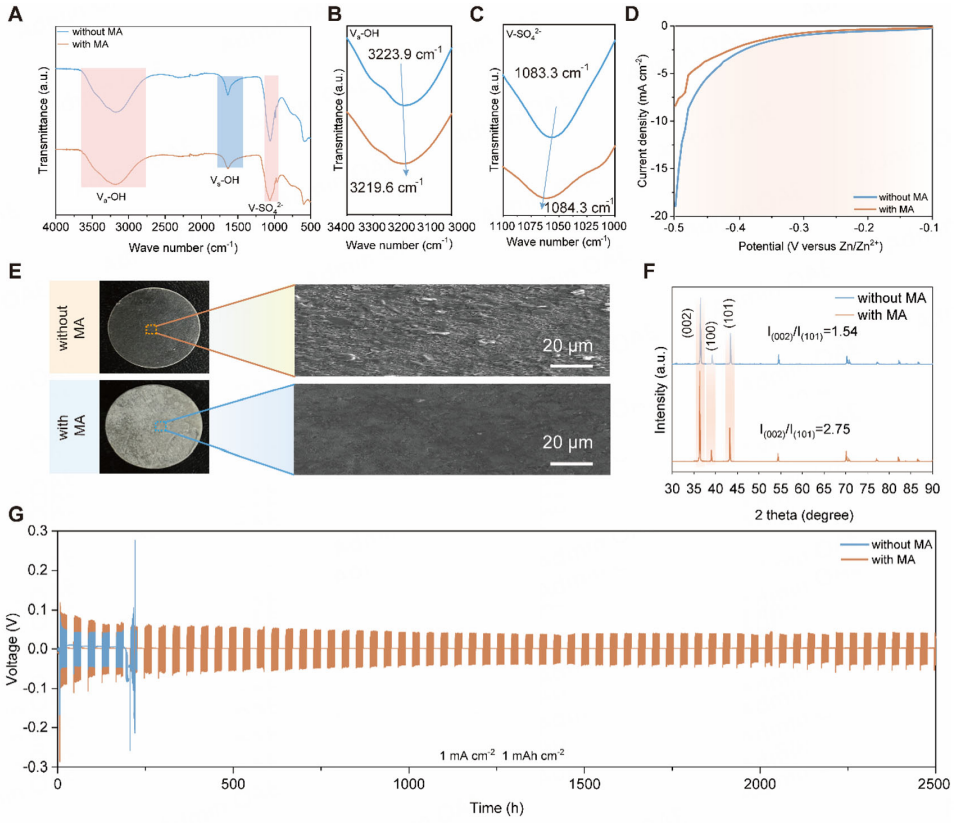

Figure 3. (A-C) FTIR spectra of different electrolytes. (D) LSV curves using $NaSO_4$ solutions with/without MA. (E) Optical images, corresponding SEM images and (F) XRD patterns of zinc electrodes after 50 cycles using various electrolytes. (G) Electrochemical performance of the symmetric cells using different electrolytes when enduring alternate cycling and resting process.

Benefiting from the significant role of MA in stabilizing the zinc metal electrode, the enhanced electrochemical performance of cells using MA-contained electrolyte can be expected. When cycled at 5 mA cm^{-2}, the symmetric battery using MA addition achieves a long cycling life reach of 600 h [Figure 4A], while the cell in blank electrolyte displays an inferior cycle stability of less than 150 h because of the short circuit resulting from the zinc dendrites. Noticeably, at a low current density of 2 mA cm^{-2}, the battery with MA can steadily operate for 1,500 h [Figure 4B]. The corresponding enlarged voltage profiles are displayed in Figure 4C, demonstrating a gradually decreasing polarization voltage, due to the continuous activation of the anode surface[46-48]. Even when cycled under a high current density with higher capacities of 10 mA cm^{-2} and 5 mAh cm^{-2}, the excellent stability of 600 h can also be realized with the effect of MA [Supplementary Figure 6]. Figure 4D and E shows the rate performance of the symmetric batteries with/without MA at different current densities from 1 to 10 mA cm^{-2}. The cell using a MA-contained electrolyte displays a steadier cycle profile with a smaller polarization voltage than that in the blank electrolyte. Furthermore, the limit capacity tests, conducted through a set deposition/dissolution duration of 1 h and a progressive increase in current density by 0.2 mA cm^{-2}, also highlight the electrochemical reversibility in the MA-containing electrolyte [Supplementary Figure 7]. These findings further confirm that the interfacial preferentially adsorbed MA can create an adsorption layer on Zn interface, which efficiently prevents zinc dendrite formation and parasitic side reactions, thereby markedly improving the reversibility and stability of zinc electrodes.

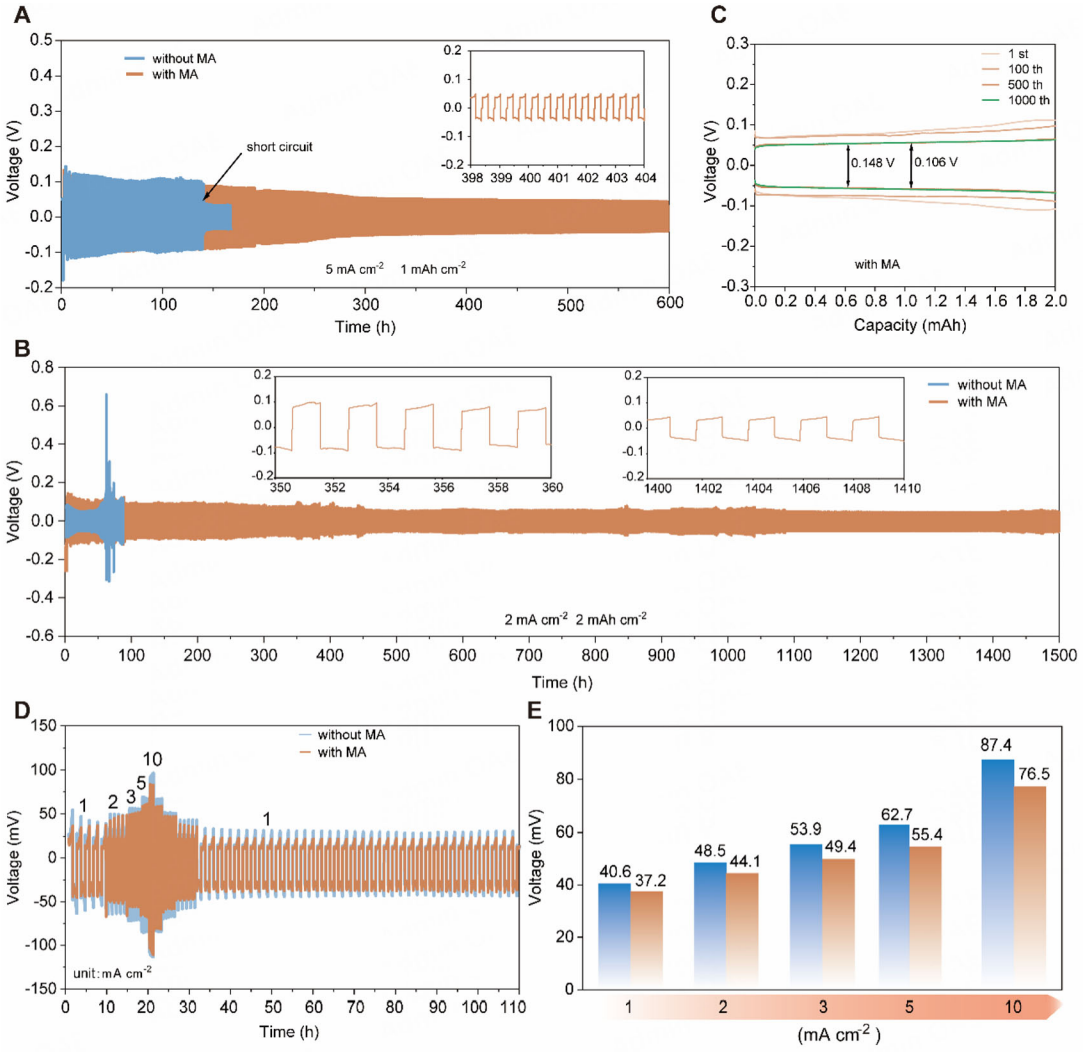

Figure 4. (A) Current-voltage profiles of the Zn//Zn symmetrical batteries with different electrolytes at 5 mA cm^{-2} with 1 mAh cm^{-2}. (B) Enlarged voltage profiles of the symmetrical cell. (C) Current-voltage profiles of symmetrical cells with different electrolytes at 2 mA cm^{-2} and 2 mAh cm^{-2}. (D) The rate performance of symmetrical cells with a fixed capacity of 1 mAh cm^{-2}. (E) Corresponding polarization voltage values of symmetrical cells at various current densities.

The enhanced electrochemical reversibility means an outstanding improvement in the stability of zinc electrodes, and also proves that the growth process of zinc dendrites is inhibited. The macroscale images of zinc metal deposition in different electrolytes are depicted in Figure 5A-F, showcasing a pronounced difference in the deposition morphology. In addition, the 3D confocal laser scanning microscopy (CLSM) images indicate that the Zn anode cycled in the MA-free electrolyte has a rough surface with high average surface roughness. Conversely, the anode cycled in the MA-containing electrolyte shows a markedly smoother and more compact surface, with a significantly lower average surface roughness. Furthermore, the Zn//NVO full batteries were assembled with electrolytes without/with MA to evaluate the practical application potential. Attributed to the enhanced reversibility of the zinc electrode in the MA-contained electrolyte, the Zn//NVO full cell delivers outstanding cycling stability with a high specific capacity of 138.4 mAh g^{-1} and a high capacity retention of 92.8% at 1 A g^{-1} [Figure 5G and H]. Conversely, the cell with blank electrolyte displays a fast capacity decay accompanied by a lower capacity retention of 63.2% [Figure 5G and Supplementary Figure 8], due to the uncontrolled growth of Zn dendrites in the absence of

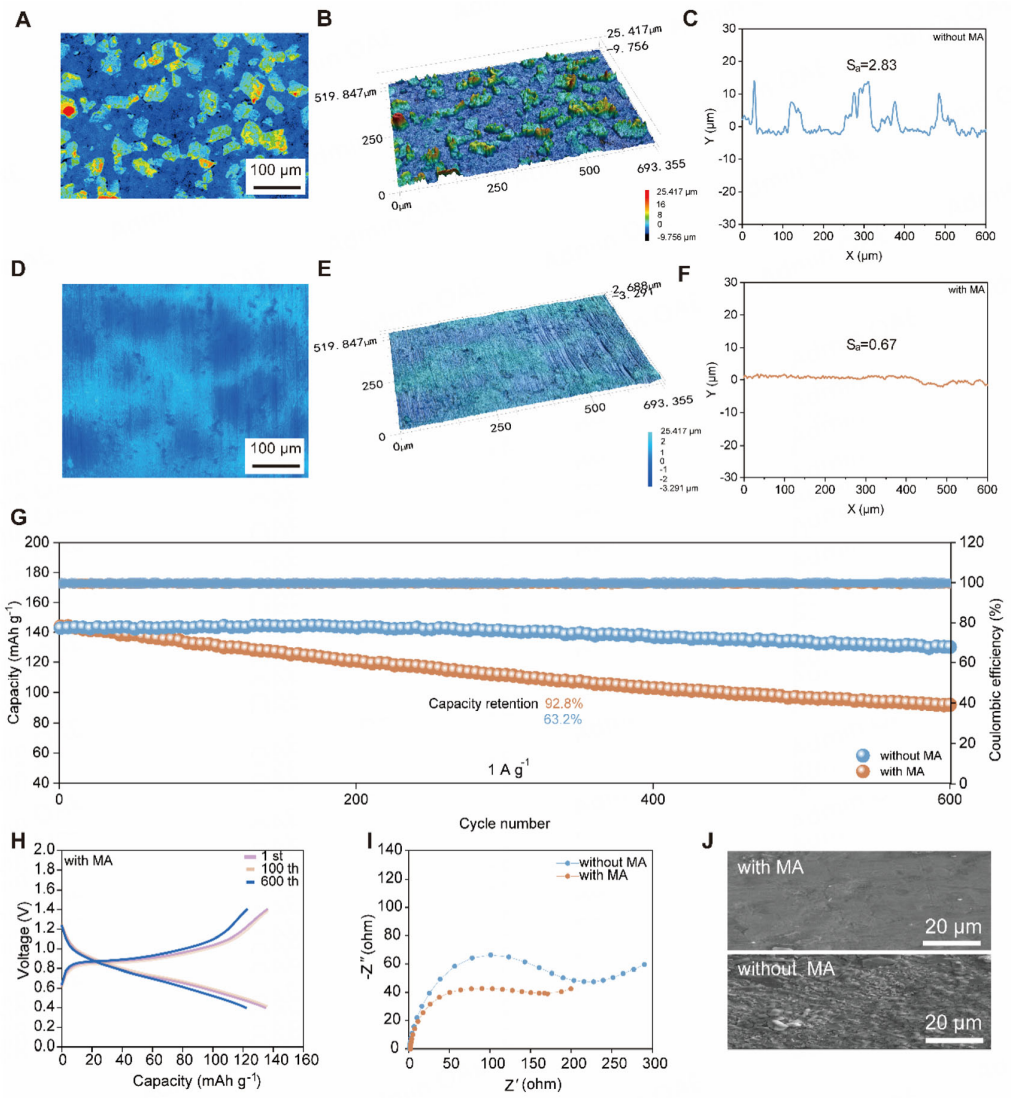

Figure 5. CLSM images and the corresponding surface roughness curve of the Zn electrodes after fifty cycles in electrolytes (A-C) without and (D-F) with MA addition. Electrochemical performance of Zn//NVO full cells using electrolytes with/without MA: (G) Cycling performance at 1 A g^{-1}; (H) Selected GCD curves; (I) EIS curves; (J) SEM images of the anodes of full batteries after 50 cycles.

MA[49,50]. Furthermore, the Zn//NVO full battery incorporating MA demonstrates a significantly reduced interface impedance, signifying excellent interfacial compatibility between the anode and the electrolyte [Figure 5I], which is beneficial for enhancing the cycling stability of full batteries[51,52]. The surface morphology of zinc electrodes after fifty cycles at 1 A g^{-1} was examined [Figure 5J]. It is evident that the zinc electrode cycled in the blank electrolyte exhibits numerous irregular dendrites and mossy Zn deposits. On the contrary, the zinc electrode cycled in the MA-contained electrolyte retains a compact and dense deposition structure without obvious corrosion pits. In addition, we assembled a Zn//I_2 full cell using iodine as the cathode. Surprisingly, the Zn//I_2 full cell can stably run for 300 cycles with a specific capacity of 3.97 mAh at a high loading of 25.4 mg cm^{-2} [Supplementary Figure 9]. The above results underscore the effectiveness of the MA additive electrolyte strategy in stabilizing the zinc metal electrode and enabling the development of high-performance AZIBs.

CONCLUSIONS

To summarize, we utilized MA with nucleophilic groups as an interface stabilizer to enhance the cycling performance of the Zn anode. Combining the calculation and experiment results, MA molecules preferentially adsorb on the Zn/electrolyte interface, owing to their strong affinity to the zinc metal anode. Moderate electron-withdrawing properties of carbonyl groups allow them to redistribute the charge, thereby modulating the nucleation and growth of Zn^{2+}, which leads to the achievement of a uniform and compact Zn deposition layer[53]. Moreover, the adsorbed MA molecules establish a H_2O-poor EDL structure which diminishes side reactions and surface passivation at the AEI due to the decomposition of active water. Consequently, the symmetric cell using MA-contained electrolyte delivers an enhanced stability of 1,500 h and promotes high Zn plating/striping reversibility over 1,400 cycles in Zn//Cu asymmetric cell at 2 mA cm^{-2}. Additionally, the Zn//NVO full cell with the incorporation of MA achieves a high capacity retention of 92.8% for 600 cycles at 1 A g^{-1}. This finding provides an efficient strategy for AEI through ester-based additives with nucleophilic groups for fulfilling highly reversible Zn anodes.

DECLARATIONS

Authors' contributions

Materials synthesis, electrochemical experiments, data collection and analysis: Li, C.
Data acquisition, visualization, and investigation: Qi, H.; Huang, J.; Chen, D.
Mechanism explanation, data acquisition, and visualization: Cheng, Y.; Xu, M.
Methodology, initial draft writing, and manuscript revision: Jiang, Z.; Yu, H.
Supervision, manuscript revision, and funding acquisition: Huang, Y.; Li, G.; Chen, Y.

Availability of data and materials

The raw data supporting the findings of this study are available within this Article and its Supplementary Materials. Further data is available from the corresponding authors upon reasonable request.

Financial support and sponsorship

This research was financially supported by the National Natural Science Foundation of China (No. 52377222) and the Natural Science Foundation of Hunan Province (No. 2023JJ20064).

Conflicts of interest

All authors declared that there are no conflicts of interest.

Ethical approval and consent to participate

Not applicable.

Consent for publication

Not applicable.

REFERENCES

1. Chen, F.; Xu, Z. L. Design and manufacture of high-performance microbatteries: lithium and beyond. *Microstructures* **2022**, *2*, 2022012. DOI
2. Hu, Y.; Wang, P.; Li, M.; Liu, Z.; Liang, S.; Fang, G. Challenges and industrial considerations towards stable and high-energy-density aqueous zinc-ion batteries. *Energy. Environ. Sci.* **2024**, *17*, 8078-93. DOI
3. Wang, Y.; Wang, Z.; Pang, W. K.; et al. Solvent control of water O-H bonds for highly reversible zinc ion batteries. *Nat. Commun.* **2023**, *14*, 2720. DOI PubMed PMC

4. Sun, D.; Sun, Z.; Yang, D.; Jiang, X.; Tang, J.; Wang, X. Advances in boron nitride-based materials for electrochemical energy storage and conversion. *EcoEnergy* **2023**, *1*, 375-404. DOI
5. Chavhan, M. P.; Kryeziu, A.; Ganguly, S.; Parmentier, J. Monolithic metal-based/porous carbon nanocomposites made from dissolved cellulose for use in electrochemical capacitor. *Green. Carbon.* **2024**, *2*, 109-17. DOI
6. Huang, S.; Li, K.; He, Z.; et al. Rolling strategy for highly efficient preparation of phosphating interface enabled the stable lithium anode. *J. Alloys. Compd.* **2024**, *1005*, 176193. DOI
7. Yang, H.; Zheng, H.; Yu, H.; et al. Coordinating ionic and electronic conductivity on 3D porous host enabling deep dense lithium deposition toward high-capacity lithium metal anodes. *Nanoscale* **2022**, *14*, 13722-30. DOI
8. Cheng, Z.; Wang, K.; Fu, J.; et al. Texture exposure of unconventional $(101)_{Zn}$ facet: enabling dendrite-free Zn Deposition on metallic zinc anodes. *Adv. Energy. Mater.* **2024**, *14*, 2304003. DOI
9. Ren, J.; Wu, H.; Yan, W.; Huang, P.; Lai, C. Stable zinc anode by regulating the solvated shell and electrode–electrolyte interface with a sodium tartrate additive. *Ind. Chem. Mater.* **2024**, *2*, 328-39. DOI
10. Wei, Z.; Zhang, H.; Li, A.; et al. Construction of in-plane 3D network electrode strategy for promoting zinc ion storage capacity. *Energy. Storage. Mater.* **2023**, *55*, 754-62. DOI
11. Bai, Y.; Deng, D.; Wang, J.; et al. Inhibited passivation by bioinspired cell membrane Zn interface for Zn-air batteries with extended temperature adaptability. *Adv. Mater.* **2024**, *36*, e2411404. DOI
12. Wang, D.; Li, R.; Dong, J.; et al. Bidentate coordination enables anions-regulated solvation structure for advanced aqueous zinc metal batteries. *Angew. Chem. Int. Ed.* **2025**, *64*, e202414117. DOI
13. Zhou, J.; Yu, H.; Qing, P.; et al. Interfacial double-coordination effect reconstructing anode/electrolyte interface for long-term and highly reversible Zn metal anodes. *J. Colloid. Interface. Sci.* **2025**, *678*, 772-82. DOI
14. Deng, S.; Xu, B.; Zhao, J.; Fu, H. Advanced design for anti-freezing aqueous zinc-ion batteries. *Energy. Storage. Mater.* **2024**, *70*, 103490. DOI
15. Zhou, J.; Zhang, L.; Peng, M.; et al. Diminishing interfacial turbulence by colloid-polymer electrolyte to stabilize zinc ion flux for deep-cycling Zn metal batteries. *Adv. Mater.* **2022**, *34*, e2200131. DOI
16. Huang, R.; Zhang, J.; Wang, W.; et al. Dual-anion chemistry synchronously regulating the solvation structure and electric double layer for durable Zn metal anodes. *Energy. Environ. Sci.* **2024**, *17*, 3179-90. DOI
17. Liu, W.; Liu, X.; Ning, F.; et al. Fabrication of a heterovalent dual-cation pre-embedded hydrated vanadium oxide cathode for high-performance zinc ion storage. *J. Mater. Chem. A.* **2024**, *12*, 11883-94. DOI
18. Ma, G.; Yuan, W.; Li, X.; et al. Organic cations texture zinc metal anodes for deep cycling aqueous zinc batteries. *Adv. Mater.* **2024**, *36*, e2408287. DOI
19. Zhang, M.; Li, S.; Tang, R.; et al. Stabilizing Zn/electrolyte interphasial chemistry by a sustained-release drug inspired indium-chelated resin protective layer for high-areal-capacity Zn//V_2O_5 batteries. *Angew. Chem. Int. Ed.* **2024**, *63*, e202405593. DOI
20. Li, J.; Lou, Y.; Zhou, S.; et al. Intrinsically decoupled coordination chemistries enable quasi-eutectic electrolytes with fast kinetics toward enhanced zinc-ion capacitors. *Angew. Chem. Int. Ed.* **2024**, *63*, e202406906. DOI
21. Chen, R.; Zhang, W.; Guan, C.; et al. Rational design of an in-situ polymer-inorganic hybrid solid electrolyte interphase for realising stable Zn metal anode under harsh conditions. *Angew. Chem. Int. Ed.* **2024**, *63*, e202401987. DOI PubMed PMC
22. Shang, Y.; Tong, Z.; Kundu, D. Decoding the zinc depletion-mediated failure in aqueous zinc batteries: on limiting parameters and accurate assessment. *ACS. Energy. Lett.* **2024**, *9*, 3084-92. DOI
23. Qu, W.; Wen, C.; Chen, B.; Cai, Y.; Zhang, M. Sulfonate-functionalization in Zn-iodine batteries as one stone kills two birds: iodine limiter and uniform Zn plating guidance layer. *Sci. China. Mater.* **2024**, *67*, 2889-97. DOI
24. Yu, H.; He, Z.; Chen, D.; et al. Zwitterionic materials for aqueous Zn-based energy storage devices: current developments and perspective. *Energy. Rev.* **2025**, *4*, 100107. DOI
25. Zha, Z.; Sun, T.; Li, D.; Ma, T.; Zhang, W.; Tao, Z. Zwitterion as electrical double layer regulator to in-situ formation of fluorinated interphase towards stable zinc anode. *Energy. Storage. Mater.* **2024**, *64*, 103059. DOI
26. Wang, L.; Yu, H.; Chen, D.; et al. Steric hindrance and orientation polarization by a zwitterionic additive to stabilize zinc metal anodes. *Carbon. Neutral.* **2024**, *3*, 996-1008. DOI
27. Li, Z.; Shu, Z.; Shen, Z.; et al. Dissolution mechanism for dendrite-free aqueous zinc-ions batteries. *Adv. Energy. Mater.* **2024**, *14*, 2400572. DOI
28. Wei, T.; Ren, Y.; Wang, Y.; et al. Addition of dioxane in electrolyte promotes (002)-textured zinc growth and suppressed side reactions in zinc-ion batteries. *ACS. Nano.* **2023**, *17*, 3765-75. DOI
29. Li, T. C.; Lin, C.; Luo, M.; et al. Interfacial molecule engineering for reversible Zn electrochemistry. *ACS. Energy. Lett.* **2023**, *8*, 3258-68. DOI
30. Liu, D.; Zhang, Y.; Liu, S.; et al. Regulating the electrolyte solvation structure enables ultralong lifespan vanadium-based cathodes with excellent low-temperature performance. *Adv. Funct. Mater.* **2022**, *32*, 2111714. DOI
31. Jiang, P.; Du, Q.; Shi, M.; Yang, W.; Liang, X. Stabilizing zinc anodes by a uniform nucleation process with cysteine additive. *Small. Methods.* **2024**, *8*, e2300823. DOI
32. Liu, M.; Yuan, W.; Ma, G.; et al. In-Situ integration of a hydrophobic and fast-Zn^{2+}-conductive inorganic interphase to stabilize Zn metal anodes. *Angew. Chem. Int. Ed.* **2023**, *62*, e202304444. DOI
33. Zong, W.; Li, J.; Zhang, C.; et al. Dynamical Janus interface design for reversible and fast-charging zinc-iodine battery under extreme

operating conditions. *J. Am. Chem. Soc.* **2024**, *146*, 21377-88. DOI

34. Zhang, C.; Li, C.; Chen, D.; et al. Zn^{2+} flux regulator to modulate the interface chemistry toward highly reversible Zn anode. *J. Colloid. Interface. Sci.* **2025**, *682*, 232-41. DOI
35. Zhao, R.; Dong, X.; Liang, P.; et al. Prioritizing hetero-metallic interfaces via thermodynamics inertia and kinetics zincophilia metrics for tough Zn-based aqueous batteries. *Adv. Mater.* **2023**, *35*, e2209288. DOI
36. Kong, W.; Wan, F.; Lei, Y.; et al. Dynamic detection of decomposition gases in eco-friendly $C_5F_{10}O$ gas-insulated power equipment by fiber-enhanced Raman spectroscopy. *Anal. Chem.* **2024**, *96*, 15313-21. DOI
37. Zhao, Q.; Liu, W.; Ni, X.; et al. Steering interfacial renovation with highly electronegative Cl modulated trinity effect for exceptional durable zinc anode. *Adv. Funct. Mater.* **2024**, *34*, 2404219. DOI
38. Cao, J.; Wu, H.; Zhang, D.; et al. In-situ ultrafast construction of zinc tungstate interface layer for highly reversible zinc anodes. *Angew. Chem. Int. Ed.* **2024**, *63*, e202319661. DOI
39. Peng, M.; Tang, X.; Xiao, K.; Hu, T.; Yuan, K.; Chen, Y. Polycation-regulated electrolyte and interfacial electric fields for stable zinc metal batteries. *Angew. Chem. Int. Ed.* **2023**, *62*, e202302701. DOI
40. Bu, F.; Gao, Y.; Zhao, W.; et al. Bio-inspired trace hydroxyl-rich electrolyte additives for high-rate and stable Zn-ion batteries at low temperatures. *Angew. Chem. Int. Ed.* **2024**, *63*, e202318496. DOI
41. Chang, C.; Hu, S.; Li, T.; et al. A robust gradient solid electrolyte interphase enables fast Zn dissolution and deposition dynamics. *Energy. Environ. Sci.* **2024**, *17*, 680-94. DOI
42. Chen, W.; Tan, Y.; Guo, C.; et al. Biomass-derived polymer as a flexible "zincophilic-hydrophobic" solid electrolyte interphase layer to enable practical Zn metal anodes. *J. Colloid. Interface. Sci.* **2024**, *669*, 104-16. DOI
43. Ma, X.; Yu, H.; Yan, C.; et al. Nitroxyl radical triggered the construction of a molecular protective layer for achieving durable Zn metal anodes. *J. Colloid. Interface. Sci.* **2024**, *664*, 539-48. DOI
44. Yuan, W.; Nie, X.; Wang, Y.; et al. Orientational electrodeposition of highly (002)-textured zinc metal anodes enabled by iodide ions for stable aqueous zinc batteries. *ACS. Nano.* **2023**, *17*, 23861-71. DOI
45. Zhu, Q.; Sun, G.; Qiao, S.; et al. Selective shielding of the (002) plane enabling vertically oriented zinc plating for dendrite-free zinc anode. *Adv. Mater.* **2024**, *36*, e2308577. DOI
46. Wang, C.; Yang, Y.; Zhang, S.; et al. The impact of surface functional groups on MXene anode protective layer in aqueous zinc-ion batteries: understanding the mechanism. *J. Energy. Storage.* **2024**, *94*, 112360. DOI
47. Li, Y.; Yang, X.; He, Y.; et al. A Novel ultrathin multiple-kinetics-enhanced polymer electrolyte editing enabled wide-temperature fast-charging solid-state zinc metal batteries. *Adv. Funct. Mater.* **2024**, *34*, 2307736. DOI
48. Yu, H.; Chen, D.; Zhang, L.; et al. Electrolyte engineering for optimizing anode/electrolyte interface towards superior aqueous zinc-ion batteries: a review. *Trans. Nonferrous. Met. Soc. China.* **2024**, *34*, 3118-50. DOI
49. Meng, C.; He, W.; Tan, H.; Wu, X.; Liu, H.; Wang, J. A eutectic electrolyte for an ultralong-lived Zn//V_2O_5 cell: an *in situ* generated gradient solid-electrolyte interphase. *Energy. Environ. Sci.* **2023**, *16*, 3587-99. DOI
50. Li, C.; Liao, T.; Chen, D.; et al. Fabrication of carbon-coated V_2O_{5-x} nanoparticles by plasma-enhanced chemical vapor deposition for high-performance aqueous zinc-ion battery composite cathodes. *Chin. Chem. Lett.* **2025**, *36*, 110557. DOI
51. Yi, X.; Fu, H.; Rao, A. M.; et al. Safe electrolyte for long-cycling alkali-ion batteries. *Nat. Sustain.* **2024**, *7*, 326-37. DOI
52. Qiu, M.; Liang, Y.; Hong, J.; Li, J.; Sun, P.; Mai, W. Entropy-driven hydrated eutectic electrolytes with diverse solvation configurations for all-temperature Zn-ion batteries. *Angew. Chem. Int. Ed.* **2024**, *63*, e202407012. DOI
53. Li, D.; Zhu, Y.; Cheng, L.; et al. A MXene modulator enabled high-loading iodine composite cathode for stable and high-energy-density Zn-I_2 battery. *Adv. Energy. Mater.* **2024**, 2404426. DOI